Quantum Electronics **51** (8) 692–699 (2021)

https://doi.org/10.1070/QEL17464

Parametric amplification in optical fibre with longitudinally varying dispersion

Yu.A. Mazhirina, L.A. Mel'nikov, A.A. Sysoliatin, A.I. Konyukhov, K.S. Gochelashvili, Deepa Venkitesh, Suchita Sarkar

Abstract. **We analyse modulation instability in fibre with longitudinally varying dispersion and the associated parametric amplification and confirm that modulation instability in such fibre is observed even in the case of positive dispersion. Highly nonlinear fibre with periodic dispersion modulation is shown to be potentially attractive as a component of a parametric amplifier with an extended gain band due to parametric resonances. Issues related to the influence of SRS and SBS on the operation of parametric amplifiers are discussed.**

Keywords: *modulation instability, dispersion varying fibre, parametric gain, gain band, stimulated Brillouin scattering.*

1. Introduction

The study of modulation instability (MI) in a nonlinear system with dispersion – Benjamin – Feir instability – has a rather long history [1, 2]. In the simplest case, this instability shows up as amplification of a weak signal having a frequency $\omega_s = \omega_p - \Omega$, detuned from the frequency of a constant amplitude pump signal, ω_p. As a consequence of four-wave nonlinear interaction, this signal undergoes parametric amplification, which converts two pump photons into signal ($\omega_s = \omega_p - \Omega$) and idler ($\omega_i = \omega_p + \Omega$) photons, their frequencies being symmetric with respect to the pump frequency. The effect shows up as amplitude modulation of light that has constant intensity at the fibre input, and subsequent breaking of the signal into a soliton pulse train [3, 4]. For the wave-matching condition to be fulfilled, the medium should have an anomalous group velocity dispersion (GVD) [1–4]. Such a parametric process can be used for signal amplification in optical fibre with an appropriate dispersion [4, 5]. In this connection, the study of MI is basic to gaining a detailed understanding of parametric amplification.

Yu.A. Mazhirina, L.A. Mel'nikov Yuri Gagarin State Technical University of Saratov, Politekhnicheskaya ul. 77, 410054 Saratov, Russia; e-mail: Lam-pels@ya.ru;
A.A. Sysoliatin, K.S. Gochelashvili Prokhorov General Physics Institute, Russian Academy of Sciences, ul. Vavilova 38, 119991 Moscow, Russia;
A.I. Konyukhov Saratov State University, Astrakhanskaya ul. 83, 410012 Saratov, Russia;
Deepa Venkitesh, Suchita Sarkar Department of Electrical Engineering, Indian Institute of Technology Madras, Chennai 6000036, ESB 337 A, India

Received 13 October 2020; revision received 9 June 2021
Kvantovaya Elektronika **51** (8) 692–699 (2021)
Translated by O.M. Tsarev

State-of-the-art communication systems use both amplitude- and phase-encoded signals. Signal amplification is ensured by semiconductor optical, erbium-doped fibre, and Raman fibre amplifiers. Standard amplifiers introduce both amplitude and phase noise into a signal. In optical fibre, matching conditions for achieving effective parametric amplification are determined by its dispersion. The use of commercially available highly nonlinear fibres for parametric signal conversion is limited by their narrow gain band and fluctuations in the zero dispersion frequency along the length of the fibre [4, 5]. In this work, we propose using modified phase-matching conditions in optical fibre with longitudinally varying dispersion [6–14], which is expected to allow one to improve the performance of such amplifiers and, possibly, implement a new signal amplification scheme for testing it under real conditions. Fibre amplifiers have an advantage over semiconductor ones because they allow for longitudinally distributed amplification and are easy to integrate into communication links [15]. We propose modifying the dispersion properties of fibre by varying its diameter because a periodic variation in fibre diameter enables quasi-phase matching conditions to be fulfilled [7, 14]. The use of fibre with periodically modulated dispersion allows one to effectively control the fission and generation of multisoliton pulses [16]. As shown in studies of MI in waveguides having a high delayed Kerr nonlinearity, with allowance for pulse self-steepening and third-order dispersion [17, 18], the combined effect of a delayed nonlinear response and negative nonlinearity dispersion leads to an increase in modulation gain coefficient. MI in inhomogeneous media, including those with periodic dispersion and a nonuniform gain profile, has been the subject of extensive studies [19–23]. In particular, Finot et al. [19] showed that, at a small dispersion modulation, additional MI regions emerged as a result of parametric resonances, which became suppressed with increasing modulation depth, whereas the width of the MI region near the pump frequency decreased. Similar results were obtained by Abdullaev et al. [20], who also estimated the width of additional parametric resonance regions. Aslam et al. [22] obtained analytical solutions for linear growth of instability, which allowed them to identify the most unstable modes, accurately calculate the rise in modulation amplitude, and find the applicability range of the analytical solutions. In addition, perturbation growth was shown to be sensitive to the initial perturbation and its phase. Rubenchik et al. [23] studied MI in fibre amplifiers. Armaroli and Biancalana [24] investigated the effect of fourth-order dispersion on MI. Their results show that conventional MI is suppressed at large dispersion modulation amplitudes and that, at a sufficiently large magnitude of negative fourth-

order dispersion (near zero second-order dispersion), MI sidebands merge and incomplete matching leads to the formation of instability regions at small detuning. Despite the incomplete matching, this is the main instability mechanism in such fibre, whereas regions of parametric resonances with large detuning have small gain. Guo et al. [25] studied conditions of MI development in fibre with amplification and soliton and breather generation, taking into account higher order effects by deriving Lax pairs, using the Darboux transformation, and constructing Akhmediev and Ma breathers, bound solitons, and two-breather solutions. Matera et al. [26] investigated instability effects due to periodic power variations in optical fibre links with losses and amplification. Droques et al. [27] experimentally demonstrated growth of MI regions and broadening of the instability region by more than 10 THz due to quasi-phase matching in fibre with periodic dispersion modulation.

The use of periodic modulation was shown to extend the range of resonance frequencies and flatten the gain profile [13, 14]. Moreover, MI was found in fibre with longitudinally decreasing dispersion [20]. As shown by Finot et al. [21], large-amplitude dispersion oscillations lead to splitting of MI bands into subbands, which can also be described as four-wave mixing of signals generated in instability bands.

In this paper, we first consider MI in dispersion varying fibre, examining the cases of purely periodic modulation and modulation in dispersion varying fibre. Next, we present calculated parametric gain and MI spectra for W profile fibre and fibre with a varying diameter.

2. MI in dispersion varying fibre

The propagation of a wave in nonlinear optical fibre with longitudinally varying dispersion is taken to obey the nonlinear Schrödinger equation (NLSE) [4]

$$2\mathrm{i}\frac{\partial u}{\partial z}+\sum_{n=2}D_n(z)\frac{\partial^n u}{\partial \tau^n}+2\alpha u^2u^*=0. \qquad (1)$$

Here $D_n(z)$ represents the second and higher orders of dispersion; α characterises the nonlinearity of the fibre; $u=u(z,t)$ is the optical field envelope; z is a coordinate along the fibre axis; $\tau=t-z/v_g$ is the retarded time of the pulse; $v_g=\mathrm{d}\omega/\mathrm{d}\beta$ is group velocity; and β is the propagation constant. Equation (1) has a solution for pumping in the form of a plane wave, $u(z)=A\exp(\mathrm{i}\alpha A^2z)$, where A is taken to be a real number. Also, in addition to pumping there is a side spectral (modulation) component such that $u(z,t)=A(1+\psi)$, where $\psi=x(z)\exp[\mathrm{i}y(z)]\cos(\Omega t)$ with a small amplitude ($|x|\ll A$). Substituting $u(z,t)$ into the NLSE (1) and retaining only the terms of first order in ψ, we obtain equations for x and y (modulation amplitude and phase) in the form [14]

$$\begin{aligned}&x''+R^2(z)\,x(z)-Q(z)x(z)=0,\\&y'=[\Omega^2D_2(z)+P\alpha]x(z),\end{aligned} \qquad (2)$$

where $R^2(z)=\frac{1}{4}\Omega^4D_2^2(z)+P\alpha\Omega^2D_2(z)$; $Q(z)=-D_2'(z)/D_2(z)$; $P=A^2$ is pump intensity; and Ω is the difference between the sideband and pump frequencies. If the fibre diameter varies periodically, we have

$$D_2(z)=D_0\Big(f\Big(\frac{z}{l_\mathrm{d}}\Big)+d_1\cos\Big(\kappa\frac{z}{l_\mathrm{d}}\Big)\Big).$$

Here D_0 is the group velocity dispersion parameter; d_1 is the dispersion modulation amplitude; $f(z)$ represents the dispersion profile of the fibre; κ is the dimensionless wavenumber; and l_d is the dispersion length. In this case, Eqn (2) has periodic coefficients and can be reduced to the Mathieu equation: $x''+\omega_0^2[1+h\cos(\kappa z)]x=0$ [3, 28], where $\omega_0^2=\frac{1}{4}\Omega^4D_0^2+P\alpha D_0+d_1\kappa/D_0$ is the square of the spatial dispersion variation frequency (expressed in inverse square kilometres); $\omega_0^2h=d_1[-4\kappa+D_0(2D_0+d_1)\Omega^4+4\alpha D_0P]4d_1\kappa+D_0^2(D_0\Omega^4+4\alpha D_0P)$; and $f(z)\equiv1$.

Figure 1a shows the variation of the effective frequency $\omega^2(z)=R^2(z)-Q(z)$ at $\Omega=0$, $\alpha=8$ km^{-1} W^{-1}, $P=1$ W, $D_0=-1$ ps^2 km^{-1}, $d_1=0.25$, and $\kappa=4$ (solid line) and, for comparison, the graph of the function $\cos(\kappa z/l_\mathrm{d}+\pi/2)$ (dashed line). It is seen that the effective frequency approaches the values given by $a+q\cos(\kappa z/l_\mathrm{d})$ at $a=0$ and $q=1$. It follows from the theory of Mathieu equations that, at $2\omega_0=m(\kappa/l_\mathrm{d})$, where m is an integer, there are parametric resonance regions [3] proportional to the dispersion modulation depth d_1, whose width decreases with increasing m. For modulation instability, phase-matching conditions [1–7] taking into account dispersion and the nonlinear phase shift should be fulfilled: $2\beta(\omega_\mathrm{p})+2\alpha P-\beta(\omega_\mathrm{p}-\Omega)-\beta(\omega_\mathrm{p}+\Omega)=0$. Taylor expanding the propagation constant in terms of frequency Ω, we obtain $\beta_2\Omega^2+2\alpha P=0$, where $\beta_2=\partial\beta/\partial\omega^2$. In the case of dispersion modulation, the phase-matching condition can be written in the form [14, 19–24]

$$D_0\Omega^2+\alpha P=m(\kappa/l_\mathrm{d}). \qquad (3)$$

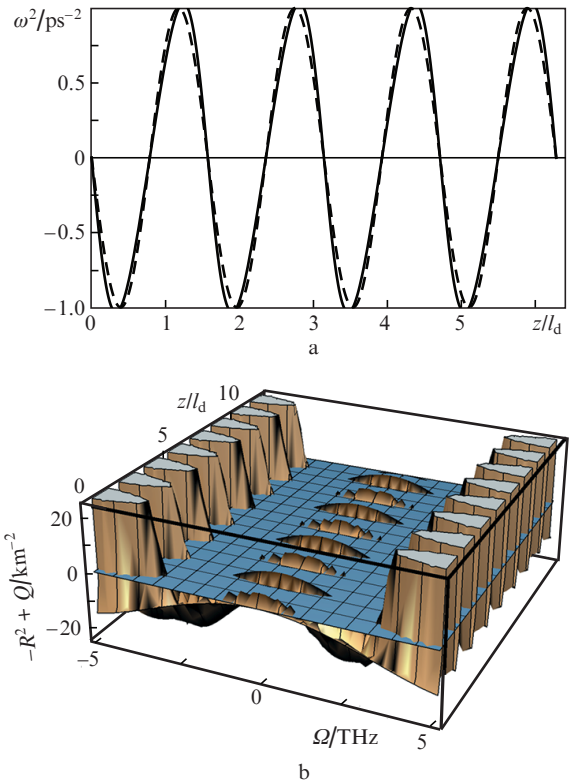

Figure 1. Square of the effective frequency $\omega^2(z)=R^2(z)-Q(z)$ in Eqn (2) (a) as a function of coordinate z/l_d and (b) as a function of z/l_d and modulation perturbation frequency Ω. In panel a, the solid line represents $\omega^2(z/l_\mathrm{d})$ and the dashed line shows the function $\cos(\kappa z/l_\mathrm{d}+\pi/2)$.

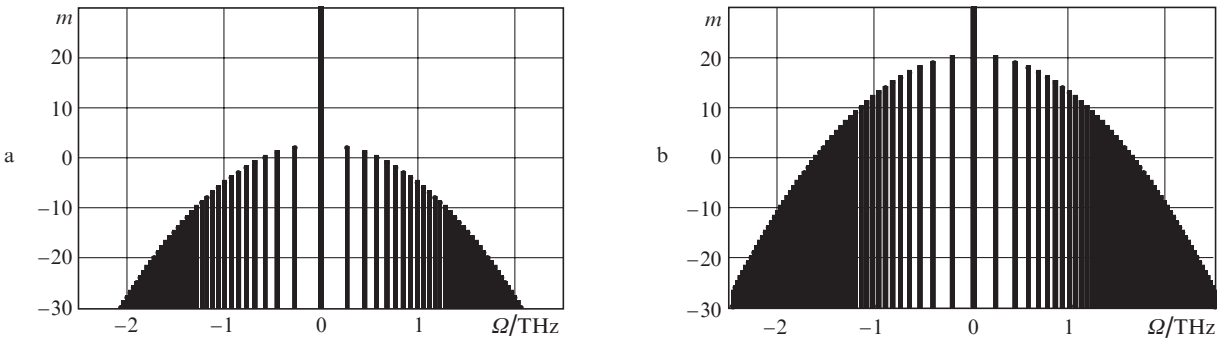

Figure 2. Modulation frequencies at which phase-matching conditions are fulfilled at $D_0 = -12$ ps^2 km^{-1}, $\kappa = 4$, $D_0\Omega^2 + 2\alpha P = m(\kappa/l_d)$, and $\alpha P =$ (a) 2 and (b) 16 km^{-1}; m is the number of the harmonic. The dots represent the harmonics that meet the matching conditions, and the vertical bars represent modulation frequencies.

Figure 2 shows Ω values for which the phase-matching conditions are fulfilled at m from –30 to 30, $D_0 = -12$ ps^2 km^{-1}, and $\alpha P = 2$ and 16 km^{-1}. It is worth noting that negative ω^2 values lead to a small-signal gain at frequencies $\omega_p \pm \Omega$. It follows from the relation for $\omega^2(z)$ that it is negative at low dispersion due to the Q term, as seen in Fig. 1b.

Figure 1b shows, in addition to the frequency $-\omega^2 = -[R^2(z) - Q]$, the $\omega^2 = 0$ plane (shown blue). Note that, for $-\omega^2 > 0$, the modulation amplitude $x(z)$ rises, which corresponds to the MI regime. Thus, MI would be expected to be observed in the frequency ranges $1 < |\Omega| < 3$ THz. At $\kappa = 4$, the solution to equation (2) has a period $l_d\pi/2$. We define the increment of modulation perturbation growth, or the MI gain, as

$$g = \frac{2}{z_0 \ln[x(z_0)/x(0)]}, \tag{4}$$

where z_0 is a sufficiently large propagation distance (in numerical calculations, we took $z_0 = 4l_d$).

Figure 2 shows the modulation frequencies at which the phase-matching condition (3) is fulfilled.

To calculate the increment of modulation perturbation growth, we numerically solved Eqns (2) at a given detuning of the modulation frequency Ω and a small amplitude of the initial perturbation [$x(0) = 0.001$] over a length $0 < z < 4l_d$. Next, using (4) we calculated the MI increment. If the modulation depth increases, the increment is positive. The frequency ranges where this occurs correspond to the MI region, and parametric amplification is possible in them. Figure 3 shows the MI increment calculated for various pump parameters and dispersion profiles with and without dispersion modulation. In the case of fibre having anomalous dispersion that is constant along its length (Fig. 3a), there are usual instability bands in the frequency range $-2.5 < \Omega < 2.5$ THz, i.e. the gain bandwidth is about 5 THz. A change in dispersion law when the dispersion profile is $D_2(z) = D_0\text{sech}(z/l_d)$ leads to a change in the shape of the MI region, whereas its width remains unchanged. Figure 3b shows the MI spectrum at this dispersion profile and simultaneous modulation. For $|\Omega| > 2.4$ THz, additional instability bands emerge at the additional frequencies given by (3), and the width of the instability region increases markedly. Figure 3c shows the instability spectrum at a $D_0\text{sech}(z/l_d)$ dispersion profile and modulation of the form $0.75\cos(4z^2/l_d^2)$. In this case, there are also additional instability bands, which leads to an increase in the total linewidth to almost 12 THz. The position of these additional bands correlates well with the frequencies in Fig. 2. Figure 3d shows the spectrum obtained in the case of chirped dispersion modulation with a $D_0(\text{sech}(vz/l_d) + d_1\cos(z/l_d)^2)$ profile. There are also additional instability bands, but they overlap, so the spectrum is less jagged. Increasing the pump intensity also leads to smoothing of the spectrum (Fig. 3e), which becomes ever smoother with increasing pump intensity. Thus, if modulated dispersion fibre is used as a parametric amplifier, it is reasonable to have fibre with varying (decreasing) dispersion and chirped modulation and use an increased pump intensity. It is then expected that the calculated gain over a fibre length of four dispersion lengths (in the case of fibre with $D_0 = -12$ ps^2 km^{-1} and a pulse duration of 1 ps, $4l_d$ corresponds to a fibre length of 330 m) is about 30 dB.

At a low level of pumping, the parametric resonance regions are well separated, but with increasing pump intensity they overlap to a significant degree, which is essential for parametric amplification because amplification at separate resonance frequencies leads to distortion of the pulse shape. Thus, to ensure the parametric amplification regime, it is necessary to adjust the fibre dispersion profile, the level of pumping, and the modulation depth. Note that, from the shape of the frequency dependence of the MI increment, one can assess distortion of the pulse shape. It is easy to show that the amplified signal spectrum $S_{out}(\Omega, z)$ can be obtained by multiplying the spectrum of the signal at the amplifier input by the gain spectrum:

$$S_{out}(\Omega, z) = S(\Omega)\exp\left[\int_0^z dz' g(\Omega, z')\right]. \tag{5}$$

We plan to present pulse shape distortion calculation results in a separate report.

Figure 4 shows MI regions calculated with allowance for only second-order dispersion terms (Fig. 4a) and for up to the fifth order of dispersion (Fig. 4b). Comparison of these data demonstrates that taking into account higher order dispersion terms leads to asymmetry of amplification regions (Fig. 4b), whereas their width remains essentially unchanged.

3. Calculation of dispersion in W profile fibre

Dispersion in W profile fibre was calculated by a standard method [29]. The refractive index profile (RIP) of such fibre is shown in Fig. 5. To obtain its dispersion relation, we used expressions for the LP mode field in the fibre core (I), trench (II), and cladding (III) in the form

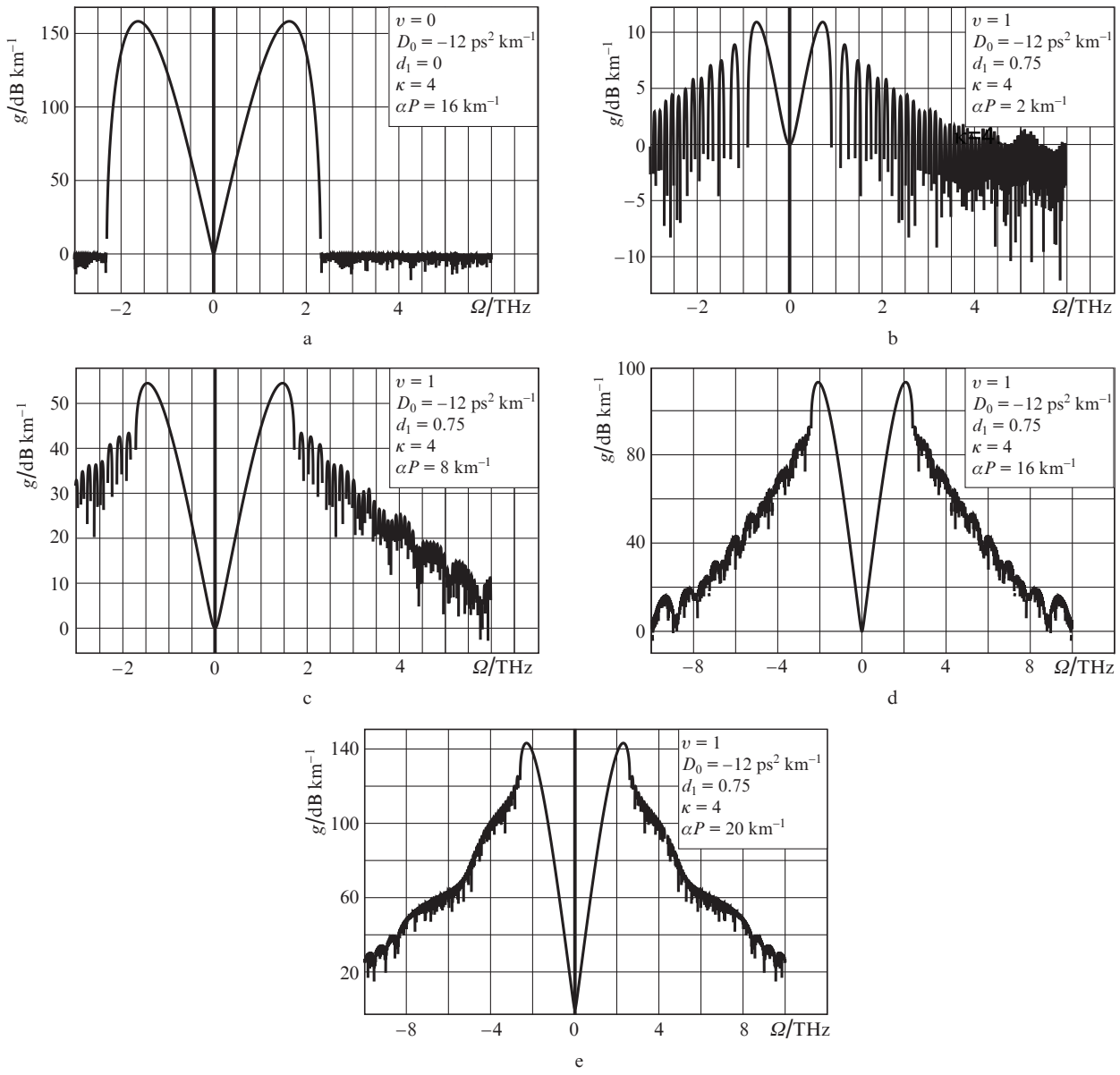

Figure 3. MI regions in fibres with (a) constant dispersion, (b) decreasing dispersion, (c, d) modulated decreasing dispersion, and (e) decreasing dispersion and increasing dispersion modulation amplitude. The dispersion profile of the fibre is (a, b) $D_2(z) = D_0(\mathrm{sech}(vz/l_\mathrm{d}) + d_1\cos(\kappa z/l_\mathrm{d}))$, (c, d) $D_2(z) = D_0(\mathrm{sech}(vz/l_\mathrm{d}) + d_1\cos[\kappa(z/l_\mathrm{d})^2])$, and (e) $D_2(z) = D_0(\mathrm{sech}(vz/l_\mathrm{d}) + d_1 z(4l_\mathrm{d})^{-1}\cos(\kappa z/l_\mathrm{d}))$.

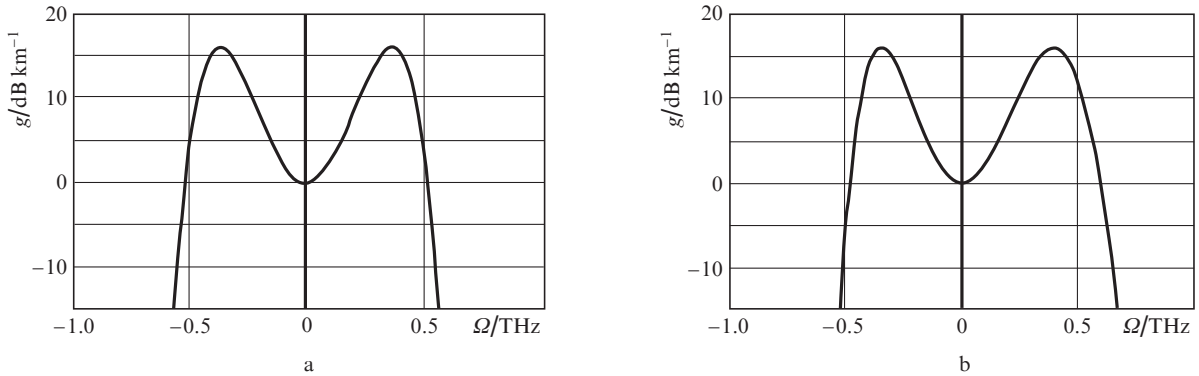

Figure 4. MI regions at the following dispersion parameters: (a) $D_2 = 1$ ps^2 km^{-1}, $D_3 = 0$, $D_4 = 0$, $D_5 = 0$, $\alpha P = 4$ km^{-1}; (b) $D_2 = 1$ ps^2 km^{-1}, $D_3 = 0.1$ ps^3 km^{-1}, $D_4 = -0.1$ ps^4 km^{-1}, $D_5 = -5$ ps^5 km^{-1}, $\alpha P = 4$ km^{-1}.

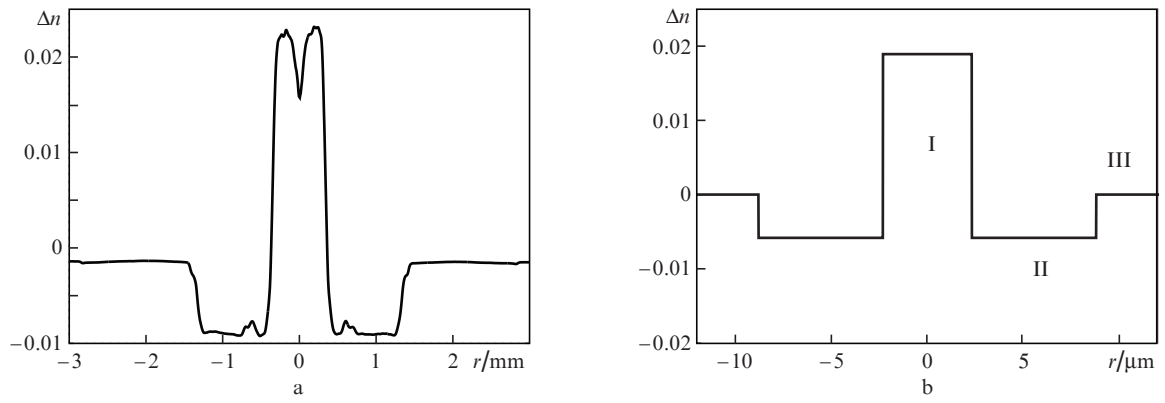

Figure 5. (a) Experimentally measured RIP of a preform at a wavelength of 633 nm and (b) the fibre RIP used in calculations; the RIP difference is $\Delta n = n(r) - n_0$.

$$\boldsymbol{E}(r,\varphi) = \boldsymbol{e}\exp(\mathrm{i}\nu\varphi + \mathrm{i}\omega t - \mathrm{i}\beta z)$$

$$\times\begin{cases} AJ_\nu(ur/a), r < a\ (\mathrm{I}), \\ BI_\nu(qr/a) + CK_\nu(qr/a), a < r < b\ (\mathrm{II}), \\ DK_\nu(wr/a), r > b\ (\mathrm{III}). \end{cases} \quad (6)$$

Here $\boldsymbol{e}$ is the wave polarisation vector; J_ν is the Bessel function; I_ν is the modified Bessel function; K_ν is the Macdonald function of order ν; a is the core radius; b is the trench radius; and u, q, and w are transverse wavenumbers. Equating the fields and the derivatives with respect to radius r across the boundaries of regions I–III (Fig. 5b), we obtain a linear system of equations in the unknown coefficients A, B, C, and D for the fundamental mode with $\nu = 0$ [29]:

$$\begin{aligned} &AJ_0(u) = BK_0(q) + CI_0(q), \\ &BK_0(wb/a) + CI_0(wb/a) = DK_0(qb/a), \\ &BK_0(wb/a) + CI_0(wb/a) = DK_0(qb/a), \\ &-wBK_1(wb/a) + wCI_1(wb/a) = -qDK_1(qb/a). \end{aligned} \quad (7)$$

This homogeneous system of linear equations should have zero determinant for the A, B, C, and D amplitudes to be nonzero. The condition that the determinant of system (7) be zero is termed the dispersion equation. Together with the relations between the transverse wavenumbers u, q, and w and the propagation constant, which have the form

$$\begin{aligned} u^2a^2 &= K^2a^2n_c^2 - \beta^2a^2, \\ -q^2a^2 &= K^2a^2n_t^2 - \beta^2a^2, \\ -w^2a^2 &= K^2a^2n_{cl}^2 - \beta^2a^2, \end{aligned} \quad (8)$$

they give four equations which allow the dispersion of the fibre to be found. Here n_c, n_t, and n_{cl} are the refractive indices of the core, trench, and cladding, respectively. To calculate the dispersion of the fibre, we used the wavelength dependence of the refractive index for GeO_2-doped silica, given by the Sellmeier formula [29]:

$$n^2_{GeO_2}(X,\lambda) = 1 + \sum \frac{\lambda^2(A_j + XG_j)}{\lambda^2 - (l_j + Xlg_j)^2}. \quad (9)$$

Here X is the relative GeO_2 content, such that $0 < X < 1$; $X = 0$ corresponds to undoped SiO_2. The parameters of this relation are given in Table 1.

Table 1. Data for calculation of the refractive index of GeO_2-doped SiO_2.

Parameter	$j = 1$	$j = 2$	$j = 3$
A_j	0.696166300	0.40794260	0.89747940
G_j	0.806866420	0.71815848	0.85416831
l_j/μm	0.068404300	0.11624140	9.89616100
lg_j/μm	0.068972606	0.15396605	11.8419310

To assess the effect of other dopants on the refractive index, we used a relation from Bruckner [30]: $n_M(X_M,\lambda) = n_{GeO_2}(0,\lambda) + \kappa_M X_M$. In calculations, we used the following coefficients κ_M for dopants M: $\kappa_M = 1.652 \times 10^{-3}$ for P_2O_5, 3.760×10^{-4} for B_2O_3, and -4.665×10^{-3} for F. In calculations of the dispersion in the fibre, the wavelength λ was varied from 0.4 to 2.5 μm in 50-nm steps. Dopant concentrations were taken such that the refractive indices at $\lambda = 633$ nm agreed with experimental data. At each value of λ, we calculated the propagation constant β and effective refractive index $n_{eff} = \beta/K$, where K is the wavenumber.

The results of dispersion calculation by fitting to the polynomial

$$n_{eff}(\lambda) = \sum_{n=0} a_n\lambda^n \quad (10)$$

are presented in Fig. 6. The coefficients a_n (in μm^{-n}) are given below:

a_0 . . . . . 2.622465357
a_1 . . . . . −2.325436548
a_2 . . . . . 14.430000000
a_3 . . . . . −71.971500000
a_4 . . . . . 266.7710
a_5 . . . . . −609.925
a_6 . . . . . −609.925
a_7 . . . . . 6326.46
a_8 . . . . . −25968.6
a_9 . . . . . 51688.4
a_{10} . . . . . −44458.8

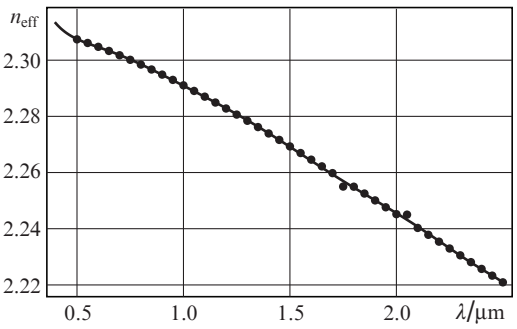

Figure 6. Calculated dispersion of W profile fibre (see Fig. 5b). The solid circles represent the calculated effective refractive index and the solid line represents the polynomial fit (10).

Using the wavelength dependence of n_{eff}, we calculated the GVD parameter (ps nm^{-1} km^{-1}) [29]:

$$\mathrm{GVD} = \frac{\lambda}{c}\frac{\partial^2 n_{\mathrm{eff}}}{\partial\lambda^2} = \frac{10^4}{3}\frac{\partial^2 n_{\mathrm{eff}}}{\partial\lambda^2}. \qquad (11)$$

The calculated dispersion agrees with experimentally measured one [16]. To calculate the $\mathrm{d}^n\beta/\mathrm{d}\omega^n$ derivatives, we used the relation between the wavelength and frequency: $\omega = 2\pi c/\lambda$. If frequency is measured in terahertz and the wavelength is measured in microns, the speed of light is c = 300 μm ps^{-1}. Since $\beta(\omega) = (\omega/c)n_{\mathrm{eff}}(\lambda)$, knowing the coefficients a_n we can calculate all the required derivatives. In particular, calculations yield $\mathrm{d}^2\beta/\mathrm{d}\omega^2 = -8$ ps^2 km^{-1}, in reasonable agreement with an experimentally determined value of –12.76 ps^2 km^{-1} [16]. At this dispersion value, the dispersion length is l_d = 62.5 m, which determines the length scale along the fibre axis z in the calculation results below. The calculated third-order dispersion parameter is $\mathrm{d}^3\beta/\mathrm{d}\omega^3 = 0.0392761$ ps^3 km^{-1}, which is of the same order as an experimentally determined value of 0.0761 pss^3 km^{-1}. Dispersion depends on the fibre core diameter. In particular, it follows from experimental data [16] that dispersion rises by 6 ps nm^{-1} km^{-1} as the fibre diameter increases by 10 μm. These data can be used in calculations of the fibre diameter profile to obtain the required dispersion profile.

An important process accompanying the propagation of a high-power wave in optical fibre is the generation of SBS components, which prevents the pump field intensity from increasing to above a certain threshold and makes it impossible to reach large parametric gain coefficients. The threshold for SBS gain is determined by its spectrum. To calculate it, it is necessary to find the profile of fibre acoustic modes and their overlap with the optical mode. The acoustic profile was calculated from the dopant concentration in the RIP of the fibre using a standard relation [1]. Acoustic profiles were determined for the RIP presented in Fig. 7a, using an acoustic velocity of 5944 m s^{-1} for the cladding [4]. Optical and acoustic equations were solved by the finite difference method in MATLAB in order to find optical and acoustic modes [2]. The calculated mode profiles were used in calculating overlap integrals of an optical and an acoustic mode to obtain the SBS gain spectrum shown in Fig. 7b. Considerable overlap of the optical and acoustic modes was only found for acoustic modes of order no greater than five (the order of the modes is indicated in the SBS gain spectrum). It is seen from Fig. 7b that SBS generation involves several acoustic modes (L_{01}–L_{02},…) and, hence, several Stokes waves are generated. Calculations were performed using a method from Refs [31, 32]. The calculation results are presented in Fig. 7.

Estimates of the SBS threshold with allowance for the data in Fig. 7b and the effective mode area of the fibre show that the threshold is 2 mW for long fibre and 2 W for short fibre. This limits the pump power to $\alpha P \approx 0.1$ km^{-1} for long fibre and $\alpha P \approx 16$ km^{-1} for short fibre.

The amplification process is accompanied by quantum noise, whose behaviour depends on the operation mode of the parametric amplifier [33, 34]. In particular, in the case of non-degenerate operation the excess quantum noise produced by the amplifier is 3 dB. In degenerate mode, the signal and idler frequencies coincide with the pump frequency ($\omega_s = \omega_i = \omega_p$), and quantum noise causes no excess noise, but there should then be phase-sensitive amplification, i.e. amplification of an in-phase signal and attenuation of a quadrature signal. In such a case, the gain coefficient depends on the phase of the signal relative to the phase of the pumping, becoming zero at a phase difference of π/2 [33]. Thus, as pointed out previously, phase-sensitive parametric amplifiers give no excess quantum noise.

In addition to SBS, SRS whose Stokes signal is redshifted from the pump frequency by about 10 THz is possible in fibre. If an amplifier operates so that the frequency of a signal wave coincides with that of the Stokes wave in the case of SRS, SRS

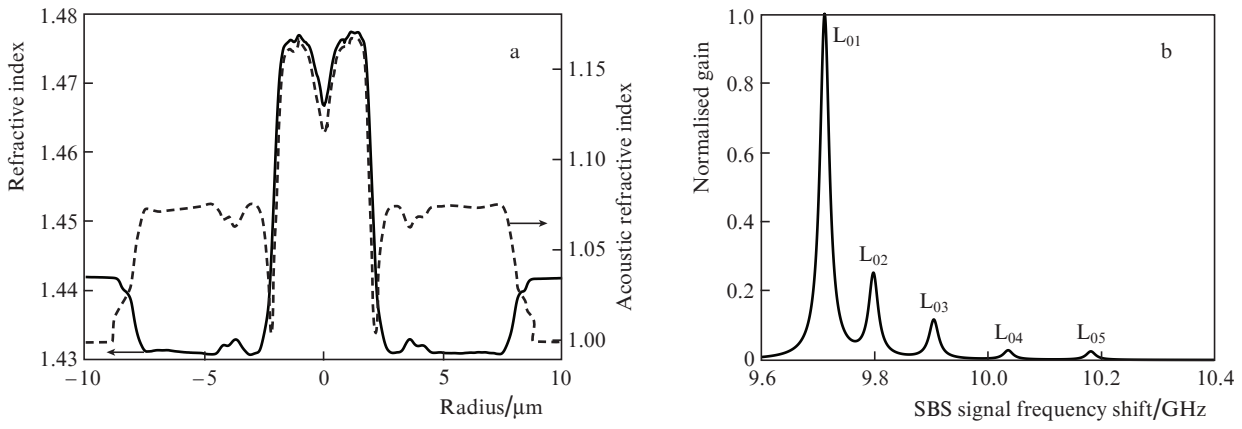

Figure 7. (a) Optical (solid line) and acoustic (dashed line) profiles of fibre and (b) calculated SBS gain spectrum of highly nonlinear W profile fibre.

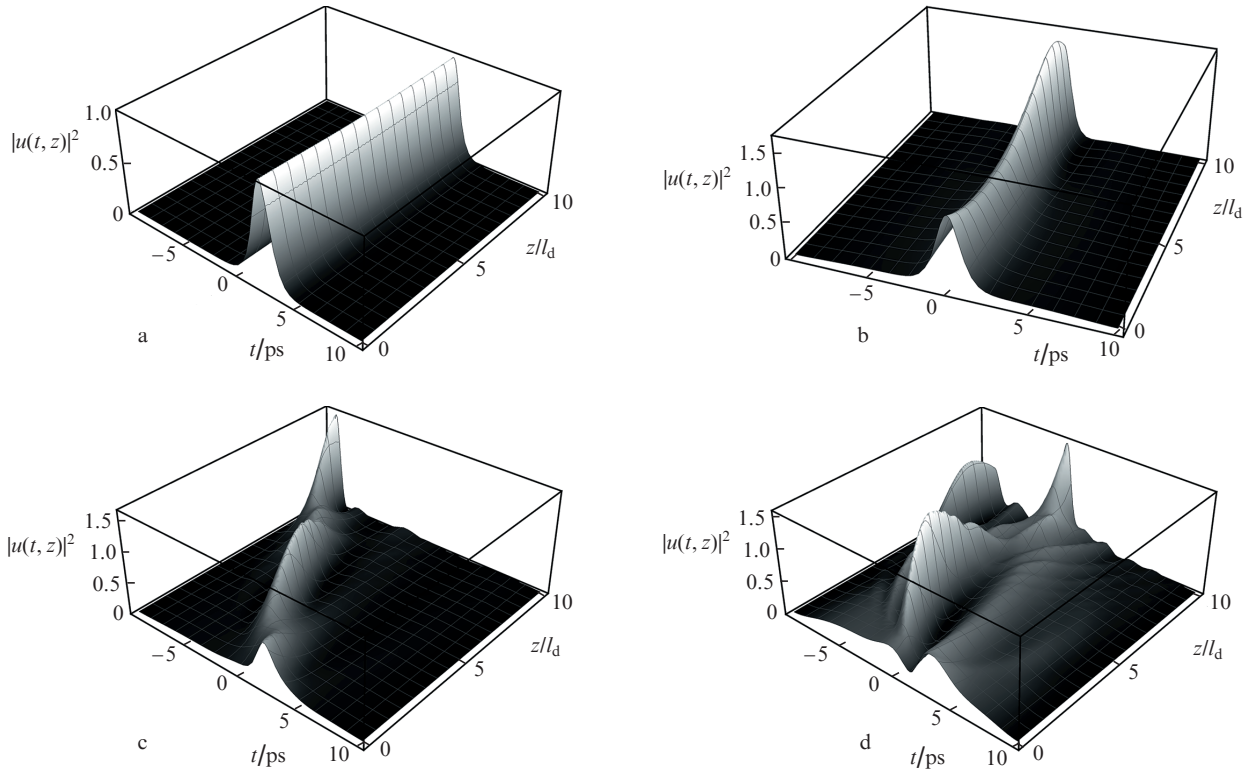

Figure 8. Spatiotemporal dynamics of the field in a degenerate case ($\Omega = 0$, $\varphi = \pi/2$, and $d_1 = 0$) in the absence of dispersion modulation and pumping ($t_0 = 2$ ps) (a), under weak pumping ($\alpha P = 0.4$ km^{-1}) (b), and in a nondegenerate case with dispersion modulation ($\Omega = 1$ THz, $\varphi = \pi/2$, and $d_1 = 0.2$) in the absence of pumping (c) and in the case of pumping ($\alpha P = 1$ km^{-1}) (d); $D_0 = -12$ ps^2 km^{-1}.

and parametric amplification compete with each other, which may lead to distortion of the signal. SRS and SBS are characterised by relaxation oscillations [8], which also distort the signal. We plan to analyse the dynamics of a parametric amplifier with allowance for both SBS and SRS in a future study.

To investigate the operation of a parametric amplifier, we modelled the propagation of a short pulse on top of a broad pump pulse. To this end, we solved the NLSE equation (1) in the range $-T < t < T$ with the initial conditions

$$u(0, t) = 1 - (t/T)^6 + a\mathrm{sech}(t + t_0)\exp(\mathrm{i}\varphi - \mathrm{i}\Omega t),$$

where $T = 20$ ps; a is the signal pulse amplitude; t_0 is the delay time; φ is the pulse phase; and Ω is the shift of the pulse frequency with respect to the pump frequency. Figure 8 illustrates the spatiotemporal dynamics of the field. In a degenerate case, phase-sensitive amplification leads to oscillations of the sum of the signal and idler fields because they have identical frequencies and their phases vary during propagation. Note that, without pumping, a soliton pulse propagates without changes in its shape or amplitude (Fig. 8a), and increasing the pump intensity increases the pulse amplitude (Fig. 8b). In a nondegenerate case, a pulse corresponding to an idler wave emerges (Fig. 8c), and interference of the signal and idler pulses is seen to become more noticeable with increasing pump intensity (Fig. 8d).

4. Conclusions

Our results have been presented on various modulation instability regimes in W profile fibre. We have calculated dispersion characteristics of such fibre, the fundamental LP mode field, and the SBS gain spectrum. Taking into account the third and fourth orders of dispersion indicates that the frequency dependence of the instability increment becomes asymmetric. In the case of dispersion varying periodically along the fibre length, there are instability bands in the signal frequency–dispersion modulation amplitude plane, and modulation instability is possible at both a positive and a negative group velocity dispersion. We have demonstrated the presence of a large number of parametric resonance regions. It is worth noting that experimental data and theoretical results in a recent paper by Panyaev et al. [35] are consistent with the present results. We have discussed issues related to excess quantum fluctuations and pointed out that there are no such fluctuations in the phase-sensitive amplification regime. The dynamics of fields under such conditions, studied numerically by solving the nonlinear Schrödinger equation for a degenerate and a nondegenerate amplifier, have demonstrated significant pulse shape distortion at high pump intensity.

Acknowledgements. This work was supported by the Russian Foundation for Basic Research (Grant No. 19-52-45012).

References

1. Segur H., Henderson D.M. *Eur. Phys. J.: Spec. Top.*, **147**, 25 (2007).
2. Zakharov V.E., Ostrovsky L.A. *Phys. D*, **238**, 540 (2009).
3. Trubetskov D.I., Ryskin N.M. *Nelineinye volny* (Nonlinear Waves) (Moscow: Nauka, 2000).
4. Agrawal G.P. *Nonlinear Fiber Optics* (New York: Elsevier, 2013).
5. Marhic M.E. *Fiber Optical Parametric Amplifiers, Oscillators and Related Devices* (Cambridge: Cambridge University Press, 2007).

6. Kikuchi K., Lorattanasane C., Futami F., Kaneko S. *IEEE Photonics Technol. Lett*., **7**, 1378 (1995).
7. Smith N.J., Doran N.J. *Opt. Lett*., **21**, 570 (1996).
8. Bronski J.C., Kutz J.N. *Opt. Lett*., **21**, 937 (1996).
9. Abdullaev F., Darmanyan S., Kobyakov A., Lederer F. *Phys. Lett. A*, **220**, 213 (1996).
10. Kaewplung P., Angkaew T., Kikuchi K. *J. Lightwave Technol*., **20**, 1895 (2002).
11. Armaroli A., Biancalana F. *Opt. Express*, **20**, 25096 (2012).
12. Jones D.J., Diddams S.A., Ranka J.K., Stentz A., Windeler R.S., Hall J.L., Cundiff S.T. *Science*, **288**, 635 (2000).
13. Mazhirina Yu.A., Konyukhov A.I., Melnikov L.A. *Izv. Vyssh. Uchebn. Zaved., Ser.: Prikl. Nelineinaya Dinam*., **16**, 70 (2008).
14. Melnikov L.A., Mazhirina Yu.A. *Quantum Electron*., **47**, 1083 (2017) [*Kvantovaya Elektron*., **47**, 1083 (2017)].
15. Croussore K., Kim C., Li G. *Opt. Lett*., **29**, 2357 (2004).
16. Sysoliatin A.A., Senatorov A.K., Konyukhov A.I., Melnikov L.A., Stasyuk V.A. *Opt. Express*, **15**, 16302 (2007).
17. Zolotovskii I.O., Sementsov D.I. *Quantum Electron*., **31** (1), 50 (2001) [*Kvantovaya Elektron*., **31** (1), 50 (2001)].
18. Zolotovskii I.O., Korobko D.A., Lapin V.A. *Quantum Electron*., **44** (1), 42 (2014) [*Kvantovaya Elektron*., **44** (1), 42 (2014)].
19. Finot C., Sysolyatin A., Wabnitz S. *Opt. Commun*., **348**, 24 (2015).
20. Abdullaev F.Kh., Darmanyan S.A., Garnier J., in *Progress in Optics* (Elsevier Science, 2002) Vol. 44, ch. 5.
21. Finot C., Feng F., Chembo Y., Wabnitz S. *Opt. Fiber Technol*., **20**, 513 (2014).
22. Aslam M.S., Hamza M.Y., Sarwar N. *AIP Adv.*, **2**, 022168 (2012).
23. Rubenchik A.M., Turitsyn S.K., Fedoruk M.P. *Proc. SPIE*, **7914**, 791434 (2011).
24. Armaroli A., Biancalana F. *Opt. Lett*., **39**, 4804 (2014).
25. Guo R., Hao H.Q., Gu X.S. *Abstr. Appl. Anal.*, **2014**, 185654 (2014).
26. Matera F., Mecozzi A., Romagnoli M., Settembre M. *Opt. Lett*., **18**, 1499 (1993).
27. Droques M., Kudlinski A., Bouwmans G., Martinelli G., Mussot A. *Opt. Lett*., **37**, 4832 (2012).
28. Abramowitz M., Stegun I. *Handbook of Mathematical Functions. Applied Mathematics Series* (National Bureau of Standards, 1964).
29. Adams M. *An Introduction to Optical Waveguides* (New York: Wiley, 1981; Moscow: Mir, 1984).
30. Bruckner V. *Elements of Optical Networking: Basics and Practice of Optical Data Communication* (Berlin: Springer, 2011).
31. Li M.-J. et al. *Opt. Express*, **15**, 8290 (2007).
32. Suchita, Srinivasan B., Venkitesh D., in *OSA Advanced Photonics Congress (AP) 2020 (IPR, NP, NOMA, Networks, PVLED, PSC, SPPCom, SOF)*. Ed. by L. Caspani, A. Tauke-Pedretti, F. Leo, B. Yang. *OSA Technical Digest* (Optical Society of America, 2020) paper JTu3F.14.
33. Yamamoto Y., Inoue K. *J. Lightwave Technol*., **21**, 2895 (2003).
34. Haus H. *Electromagnetic Noise and Quantum Optical Measurements. Advanced Texts in Physics* (Berlin: Springer-Verlag, 2000).
35. Panyaev I.S., Stolyarov D.A., Sysolyatin A.A., Zolotovskii I.O., Korobko D.A. *Quantum Electron*., **51**, 427 (2021) [*Kvantovaya Elektron*., **51**, 427 (2021)].